arXiv:1401.0635v3 [astro-ph.SR] 10 Feb 2014

On the SW Sex-Type Eclipsing Cataclysmic Variable SDSS0756+0858

Gagik Tovmassian, Mercedes Stephania Hernandez, Diego González-Buitrago, Sergey Zharikov and Maria Teresa García-Díaz

Instituto de Astronomía, Universidad Nacional Autonoma de México, Apdo. Postal 877, Ensenada, Baja California, 22800 México

gag@astro.unam.mx

ABSTRACT

We conducted a spectroscopic and photometric study of SDSS J075653.11+085831. X-ray observations were also attempted. We determined the orbital period of this binary system to be 3.29 hr. It is a deep eclipsing system, whose spectra shows mostly single-peaked Balmer emission lines and a rather intense He II line. There is also the presence of faint (often double-peaked) HeI emission lines as well as several absorption lines, Mg I being the most prominent. All of these features point towards the affiliation of this object with the growing number of SW Sex-type objects. We developed a phenomenological model of an SW Sex system to reproduce the observed photometric and spectral features.

Subject headings: stars: individual (SDSS J075653.11+085831.8) – (stars:) binaries: eclipsing; – (stars:) binaries: spectroscopic – (stars:) novae, cataclysmic variables – stars: variables: other

1. Introduction

Cataclysmic variables (CVs) are close, interactive binaries comprised of a white dwarf and a late-type, main sequence star. The latter fills its corresponding Roche lobe and loses matter via the Lagrangian L_1 point to the more massive, compact component. In most cases, the transferred matter forms an accretion disk around the white dwarf if the former has no strong magnetic field. The observational characteristics of CVs, upon which they are normally classified, depend greatly on the orbital period of the system, the mass accretion rate, and the strength of the above-mentioned magnetic field. The orbital period reflects not only the separation of the binary components, but also the size of the Roche lobe-filling secondary and therefore its evolutionary status. In particular, CVs with periods over $\sim$ 3 hours still contain secondaries with radiative cores, and thus rely on magnetic breaking as a driving force to remove the angular momentum (Rappaport et al. 1983). Systems with periods below this 3 hr threshold contain red dwarfs, which are fully convective. The magnetic breaking then becomes negligible, halting the mass transfer. Before this happens, a significant number of CVs known as SW Sex-type are observed within the $3 \sim 4$ hr period range (Schmidtobreick 2012). The SW Sex stars were first identified by Thorstensen et al. (1991) as eclipsing systems, which show characteristics very similar to each other and quite different from other CVs. Apart from wide, non-symmetric eclipses, SW Sex stars exhibit high excitation lines as well as absorption features, shifts between eclipse and emission lines phasing, and single-peaked line profiles (unusual for eclipsing binaries) containing accretion disks (Dhillon et al. 1991; Hellier 2000; Hoard et al. 2003; Rodríguez-Gil et al. 2007a). They are also defined as nova-likes, because the high mass transfer rate helps to maintain a hot and stable accretion disk devoid of dwarf-nova-type outbursts. A detailed description and discussion of properties of SW Sex stars can be found in a number of papers from the discovery of the phenomenon

(Thorstensen et al. 1991) to the latest reviews (Rodríguez-Gil et al. 2007a; Dhillon et al. 2013).

SDSS J075653.11+085831.8 (hereinafter SDSS0756+0858) was identified as a CV by Szkody et al. (2011) from the SDSS DR7 lists. From a very limited time coverage ($\sim$ 1.5 hr) they suggested that the object may have a period around two hours and thought it could be an intermediate polar. Since they covered slightly less than the actual orbital period of the system, they probably missed the eclipse, without which a correct identification becomes very difficult. We observed the object during two seasons in 2012 and 2013 by means of spectroscopy and multi-colour photometry. We find that SDSS0756+0858 is a bona-fide member of the SW Sex stars. Here, we present the results of our observations, discuss the deduced parameters of the system and its geometry. The observations and data reduction are described in Section 2, while the results are presented and discussed in Sections 3, 4, and 5. In Section 6 we present our model of SW Sex stars and draw brief conclusions in Section 7.

2. Observations and Data Reduction

2.1. Photometry

Time-resolved photometry of SDSS 0756+0858 was obtained using the direct CCD imaging mode of the 0.84 m telescope of the Observatorio Astronómico Nacional at San Pedro Mártir (OAN SPM)[1] in Mexico. We obtained a long series of photometry in the V band and one or two orbital periods with each $UBRI$ Johnson-Cousins filter. The log of photometric observations is given in Table 1. The photometric data were calibrated using Landolt standard stars. The errors, ranging from 0.01 to 0.05 mag, were estimated from the magnitude dispersion of comparison stars with similar brightness. The light curve shows deep ($\sim$ 2 mag) and wide ($\sim$ 0.2 P_{orb}) eclipses. Outside the eclipse, the object brightness varies smoothly with superposed short-time flickering. The ingress to the eclipse is steeper than the egress. Such an eclipse shape is very common for SW Sex stars (Thorstensen et al. 1991) and was a defining feature of the class until it was later revealed that there are also non-eclipsing SW Sex stars (Rodríguez-Gil et al. 2007b).

[1] http://www.astrossp.unam.mx

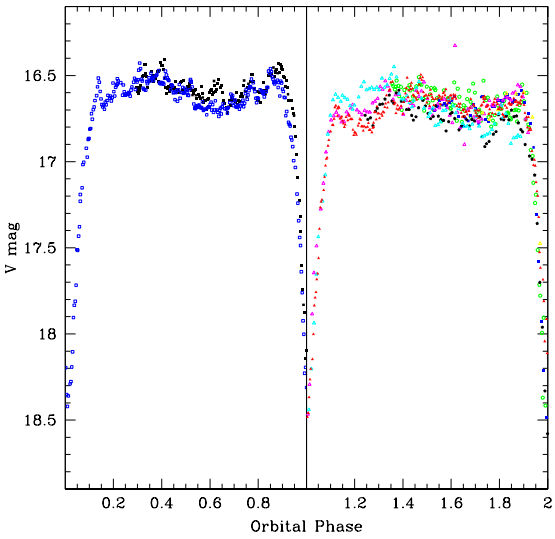

Fig. 1.— V band light curve of SDSS 0756+0858 folded with the orbital period (see Section 3). Left panel: a few orbits of V band light curves with distinct hump before the eclipse, and a pronounced dip around phase 0.6–0.7 are presented. Right panel: the rest of the light curves without the pre-eclipse hump and with a depression after the eclipse are shown.

In Figure 1, the V-band light curve, comprised of nine orbits and folded with the orbital period, is presented. The period determination is described in the next section. Two cycles are plotted to separate two distinct light curve morphologies. The left panel shows two orbits with a distinct hump before an eclipse, and a pronounced dip around phase of $\phi \sim 0.6 - 0.7$. In the right panel, the remaining light curves are combined, where the pre-eclipse hump is not so prominent and there is a distinct depression of brightness right after the eclipse. The dip around phase $\phi \sim 0.6$ is also not as defined as it is in the left panel. In both cases, the object reaches maximum brightness at phase $\phi \sim 0.4$.

2.2. Spectroscopy

We obtained long-slit spectroscopy of SDSS 0756+0858 during several observing runs using the 2.12 m telescope and the Boller & Chivens

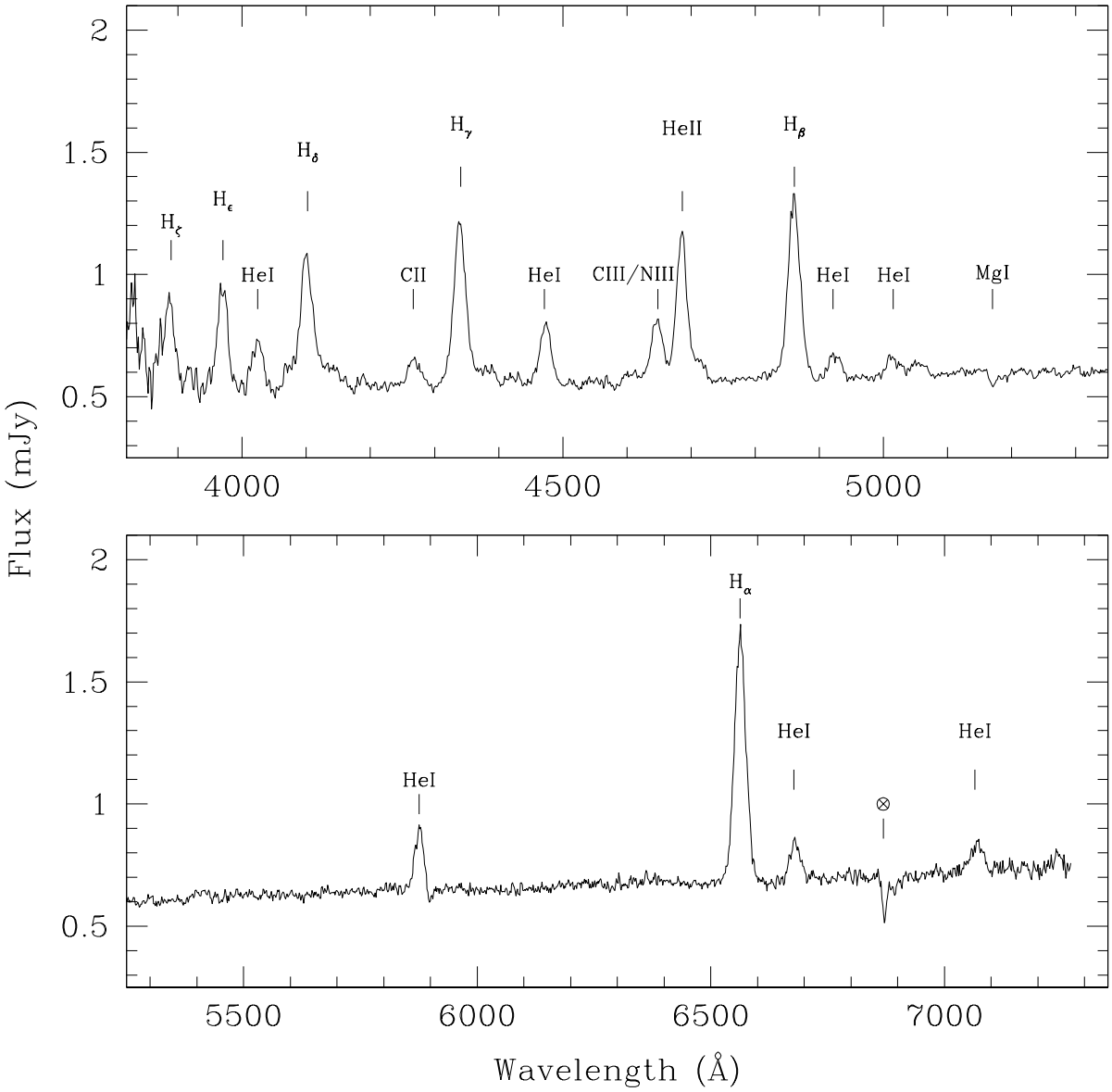

Fig. 2.— Average spectrum of SDSS 0756+0858. The major lines are marked.

spectrograph at OAN SPM. Two different gratings were used. The 1200 *l/mm* grating was used to obtain the emission line profiles with the highest possible spectral resolution (up to 2.1 Å FWHM in the covered range $\sim 4000 - 5200$ Å) in this faint $V \sim 16.25$ object. In addition, 6.5 Å resolution spectra with a higher S/N ratio were obtained with a 400 *l/mm* grating, to study the spectral energy distribution of the system, with a broader wavelength coverage ($\sim 4000 - 7200$Å). Observations were made with a 1.″5 slit, oriented in the Eeast-West direction. CuNeArg-arcs were taken every 30-40 min for wavelength calibration. The spectrograph flexions have also been checked with the night-sky lines. Spectrophotometric standards from Oke (1990) were observed each night for flux calibration. Flux losses due to the slit width and slit orientation have not been taken into account, but in some cases we have obtained simultaneous photometry and can flux-calibrate them, if necessary. The log of spectroscopic observations and the details of the instrumental setting are provided in Table 1.

The median of all 28 spectra of SDSS 0756+0858 taken on 2013 Feb 7, is presented in Figure 2. The object shows single-peaked emission lines of hydrogen (Balmer series), He I lines, He II λ 4686 Å, Bowen fluorescence C III/N III $\lambda\lambda$ 4640 − 4650 Å and C II $\lambda\lambda$4267, 7231, 7236 Å lines. Only immediately before the eclipse they show a split, which is better pronounced in the H$_\alpha$ line. He I lines show

Table 1: Log of observations

Spectrosopy† Date	Coverage hours	Resolution FWHM Å	Exposure sec
01/02/2012	7.3	2.1	600-1200
04/03/2012	5.8	4.4	600-1200
05/12/2012	1.2	2.1	900
06/12/2012	3.4	2.1	900
07/12/2012	1.5	2.1	1200
16/01/2013	2.6	2.1	1200
17/01/2013	5.4	2.1	1200
06/02/2013	3.1	6.5	600
07/02/2013	4.9	6.5	600
Photometry ††		Filter	
01/02/2012	9	V	40
03/02/2012	2.4	B/V/R/I	60-120
04/03/2012	6.2	V	60
05/03/2012	6	V	40
17/01/2013	4.0	B	90
19/01/2013	9.8	V/R	120
20/01/2013	7.6	U/I	90-120
06/02/2013	4.4	V	120
07/02/2013	5.4	V	120

† 2.12 m telescope; †† 0.84 m telescope OAN SPM

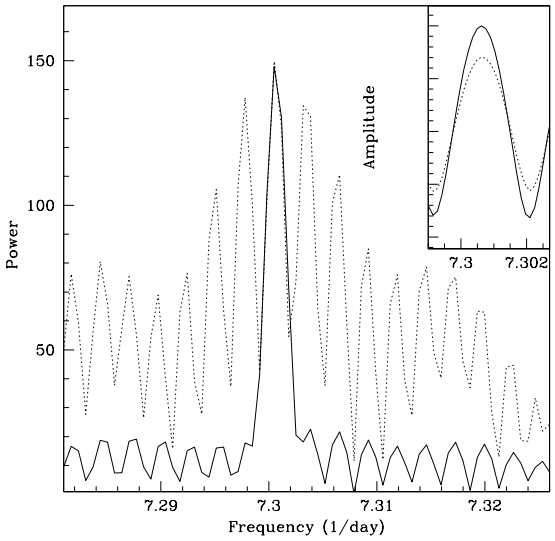

Fig. 3.— The power spectra of SDSS 0756+0858, obtained from DFT analysis. The dotted line is the spectrum obtained for H_β radial velocities. The solid line is the same after alias frequency cleaning. In the inset of the figure only the highest peak is plotted (and over-plotted is the amplitude of the power spectrum obtained from the photometry). There is excellent coincidence of frequencies, but since the amplitudes are very different the curves were scaled to fit in the same frame.

transient double peaks more often. Absorption features are also transient. The most prominent among them is the Mg line blend around λ5175 Å. The spectra taken in different epochs did not vary much in shape, therefore the spectrum in Figure 2 is representative of the object.

The parameters of spectral lines (radial velocities, intensities and FWHM) were measured by fitting a single Lorentzian to the emission lines, which describes observed profiles of lines much better (complete) than a Gaussian profile. The reason is obvious: the lines are formed in an extended area with different velocities and are wider and distorted from an instrumental profile. Often, broad emission lines of CVs are measured by so-called double Gaussian method. This procedure is very useful when dealing with the lines formed in an accretion disk and it allows one to measure velocity amplitude close to the central star. However, in this case, we do not think the lines are formed in the entire disk (see the interpretation of the system below), and therefore we did not implement this method. As an additional measure, we have repeated the analysis of lines by Gaussian fitting and no substantial differences in our results were notable.

Further discussion on spectral behavior of the object is presented below in Section 5.

2.3. X-ray observation

The *Swift* observations of SDSS 0756+0858 in November 2012 were obtained as a target of opportunity (ObsID 00045632006), prompted by the suspicion that the object is a magnetic CV (Szkody et al. 2011). The XRT data were processed with standard pipeline procedures. A 10 ks long exposure showed no detectable signal from the object (≤ 0.005 cnts/s).

3. The orbital period

The orbital period of SDSS 0756+0858 was determined on the basis of all acquired light curves

Table 2: Radial velocity fit parameters.

Line ID	γ km sec^{-1}	Velocity km sec^{-1}	Phase shift $\phi^{\dagger}$
H_α	100.2	376.8	0.88
H_β	−15.7	295.4	0.91
He II*	−18.3	191.3	0.93

* λ4686 Å

† P_{orb} and HJD_0 determined from the eclipse ephemeris.

(V band), and H_β RV variations by means of Discrete Fourier Transform (DFT), as implemented in *Period04*[2]. The resulting power spectra are presented in Figure 3. There appears to be one dominant frequency in power spectra of photometric and radial velocity data sets. As usual, they are contaminated with alias periods caused by observational cycles and frequencies of data measurement. Although the peak frequency was obvious, we analyzed the RV data for periods using *CLEAN* (Schwarz 1978), a DFT method, which convolves the power spectrum with the spectral window to eliminate alias frequencies originating from uneven data distribution. The peaks in the power spectra of photometric and radial velocity data closely coincide and correspond to the orbital period of the system.

The ephemeris deduced from the period analysis is

$$\mathrm{HJD} = 2\,455\,958.59184 + 0\overset{\mathrm{d}}{.}1369745(4) \times \mathrm{E},$$

where HJD_0 refers to the eclipse center[3]. We folded all of the V-band data with the orbital period and obtained results consistent with the curves presented in Figure 1 (with only slight differences outside eclipse. The RV curves of H_α, H_β, and He II, folded with the orbital period, are presented in Figure 4. Two thirds of spectral observations were made with the higher spectral resolution mode, but there is no notable difference in radial velocity measurements between the two sets. Least-square sinusoidal fits to the data for each emission line were calculated in the form of

$$RV(t) = \gamma + K_{em} \times \sin(2\pi\ t/P + \phi),$$

where γ is the systematic velocity, K_{em} is the semi-amplitude of radial velocity and ϕ is the zero-phase. The resulting values of γ, K_{em} and ϕ are presented in Table 2.

4. Phase dependent parameters

The eclipse profiles of SW Sex stars are usually non-symmetric and vary in shape with time (Thorstensen et al. 1991). In the case of SDSS 0756+0858 the profile has stayed fairly stable over the course of our two year monitoring. The light curve, outside the eclipse, is relatively flat. There is a small hump that appears immediately before the eclipse and a depression appears after it , as the system emerges from it (see Figure 1). The brightness then increases, peaking around $\phi = 0.4$, and experiences another depression around $\phi = 0.6 - 0.7$. This behavior is seen, generally, in all other eclipsing SW Sex stars (Thorstensen et al. 1991; Hoard et al. 1998). In addition to the long series of V photometry, we obtained multi-colour UBVRI light curves of subsequent orbital cycles (see Figure 5, left). Apparently, the pre-eclipse hump is more prominent in the blue end of the optical spectrum (B & V bands), while it is almost nonexistent in the I-band. At the same time, the eclipse depth decreases to the red. We can assume that, in eclipse, a hot source of continuum light is getting blocked by the secondary star, while the disk is not eclipsed entirely, and some cooler parts contributing in R and I bands are always visible. More telling are the variations of the emission lines parameters presented on the right side of Figure 5. In the upper panel, the intensity variation of H_α, H_β and He II lines are presented. The depth of eclipse increases with the excitation level of the line. H_α is obscured a little; its flux drops almost as much as in the counter-eclipse phase. H_β is probably produced in a more compact area and its eclipses are deeper. The high excitation line He II declines the most. The semi-amplitude of the He II RV is also significantly smaller than of the Balmer lines (Figure 4). The orbital variability of the emission line full widths (FWHM) is shown in the right, lower panel in Figure 5. Here, He II is almost flat for most orbital phases, while the Balmer lines varies greatly; the lower excitation line becoming much broader both around the eclipse and half the orbital phase.

[2] http://www.univie.ac.at/tops/Period04/

[3] (see the reference to the program for uncertainties estimate)

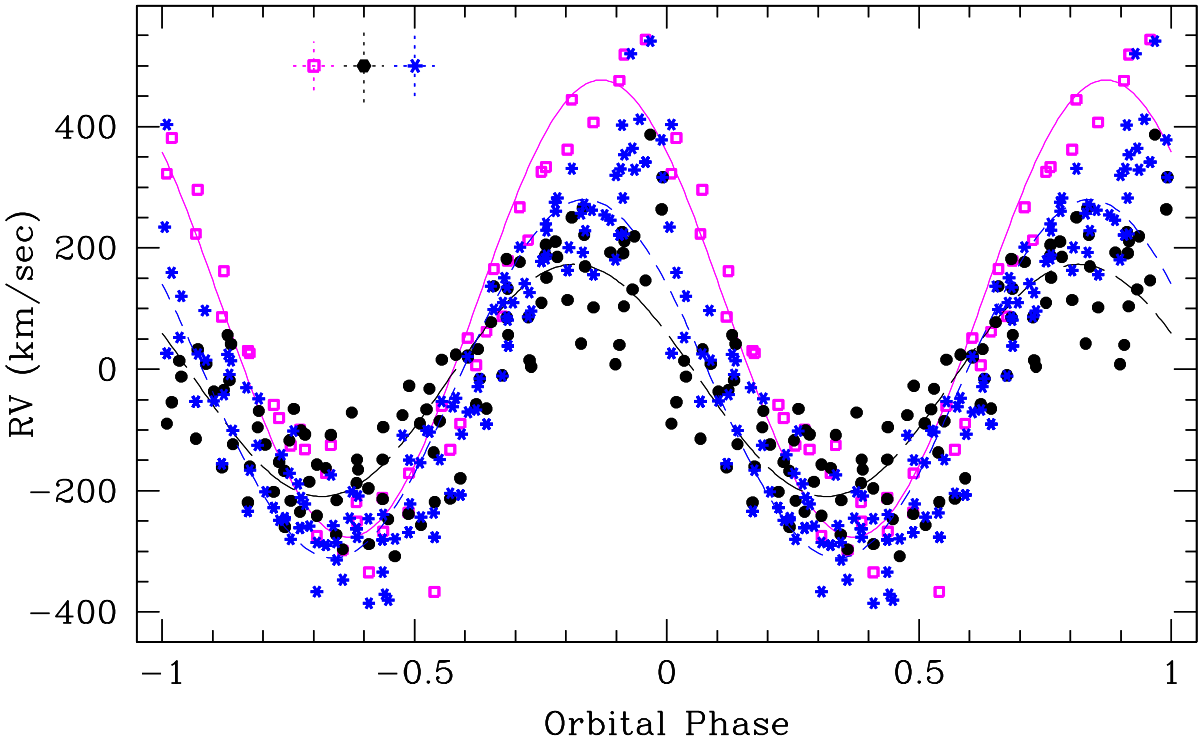

Fig. 4.— The radial velocity curves of SDSS 0756+0858. The solid black circles are measurements of the He II line and the black long-dashed line is a sinusoidal fit to the data. The blue stars and blue dashed line correspond to H_β and the magenta open squares and solid line are measurements and fit for the H_α line. All three lines show different semi-amplitude of radial velocities and phase shifts relative to each other as can be seen also from Table 2. Phase zero corresponds to the eclipse. Two orbital periods are repeated for better presentation.

The behavior of H_α, H_β, He II, He I, fluorescent emission lines C III/N III and the Mg I absorption, is depicted in a different manner by the trailed spectra in Figure 6. The trailed spectra were formed using relatively high S/N spectra obtained on two consecutive nights in February 2013. Among the features that are notable in the trailed spectra are:

- right before the eclipse (starting from $\phi = 0.8$) there is a sharp zigzag in the emission lines.
- at phase $\phi = 0$ (eclipse) there is a "tail" in emission extending to velocities exceeding 2000 km/sec.
- Balmer lines are narrower and appear more intense at phases $\phi = 0.25$ and 0.75 as demonstrated in the lower right panel of Figure 5.
- around phases $\phi = 0.4 - 0.6$ emission lines become broader, some He I lines become double-peaked. There is flaring of lines at these phases, a feature common for SW Sex objects.

Another common feature of SW Sex stars is the appearance in their spectra of the absorption lines not associated with the secondary. We can see that the Mg I "b" line appears in almost all phases, but becomes more visible around phase $\phi = 0.45 \pm 0.2$. It is also the phase when the emission lines become broader, probably due to a high velocity component and flaring. He I line practically splits at that phase.

5. Discussion

This new CV, discovered by the SDSS, exhibits all of the attributes necessary for it to be classified as a SW Sex star. It has a 3.29 hr orbital period placing it in the middle of the SW Sex stars period distribution, next to DW UMa, a classical representative of the class with which it shares many common features, as outlined by Araujo-Betancor et al. (2003); Dhillon et al. (2013). Two other similar systems, 2MASS

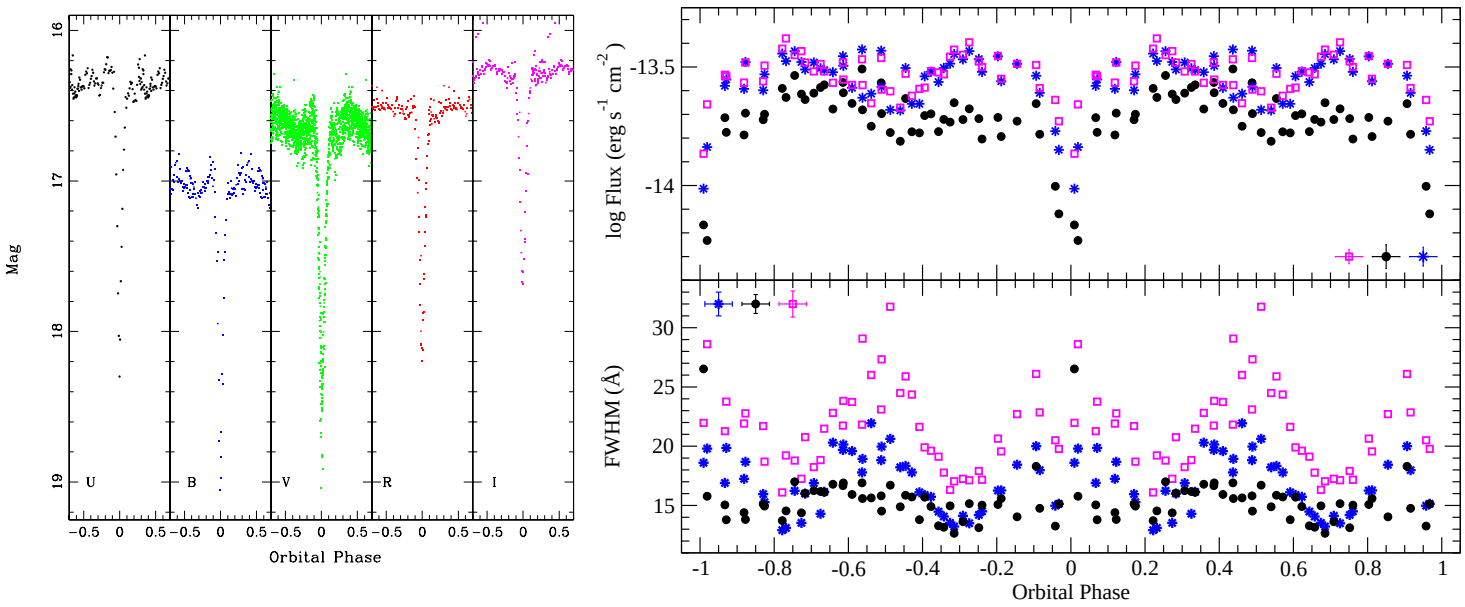

Fig. 5.— UBV*RI* light curves of SDSS 0756+0858 (left). Line parameters of SDSS 0756+0858 (right). In the upper panel, the fluxes of He II (black), H_β (blue) and H_α (magenta) emission lines are plotted versus orbital phase. In the lower panel, full width at half maximum measurements of same lines are presented. The Balmer lines show a much larger broadening around phase 0.5 than He II. At the same time, He II shows deeper eclipses than the lower excitation lines. For the sake of clarity, in the right panel the data are repeated to cover two orbital periods.

J01074282+4845188 and HBHA 4705-03 have been discovered recently (Khruzina et al. 2013; Yakin et al. 2013, although the latter is not recognized as a SW Sex star), and are not yet included in the *big-list* of SW Sex objects compiled by Hoard[4]. But the number of CVs in the $\sim 3-4$ hours orbital range bearing characteristics of SW Sex stars grows, and curiously, the fraction of eclipsing systems among SW Sex type grows too, although we are far from understanding the phenomenon itself. Besides the *V*-shaped and non-symmetric eclipses, SDSS 0756+0858 shows high velocity and single peaked emission lines forming a characteristic "S-wave" with phase shifts between different lines (Figure 4). Even the lowest measured radial velocity amplitude encountered in He II ($\sim$ 200km/s) is too high to be ascribed to the orbital velocity of a white dwarf in a CV with a three-and-half-hour orbital period. Such systems would normally consist of an 0.6–0.7$M_\odot$ white dwarf and a $0.25 \pm 0.05\,M_\odot$ secondary, with a maximum RV semi-amplitudes for the white dwarf and the secondary star reaching $\sim$ 100 and $\sim$ 300 km/sec, respectively. Otherwise, the system should contain either an abnormally light-weighted white dwarf, or an unrealistically massive secondary star.

The single-peaked emission lines remain most baffling features of SW Sex stars. Most authors employ models that help to elevate the ionized matter above the orbital plane to explain the formation of such line profiles, i.e bright-spot overflow plus accretion disc wind (Honeycutt et al. 1986; Hoare 1994; Dhillon & Rutten 1995), magnetic accretion column (Williams 1989), or magnetically driven outflow (Tout et al. 1993; Wynn & King 1995). These maybe not be necessary, if we take a clue from the study of BT Mon, an old nova with a full range of SW Sex observational characteristics, by White et al. (1996). These authors show that the emission lines originate where the bright spot should be (or slightly further), yet they claim they do not see the presence of an accretion disk. Let us keep in mind that SW Sex stars are high mass transfer rate systems and they have steady hot disks similar to those of dwarf novae in outburst (Szkody et al. 1990). Such disks are optically thick and maintain a delicate balance of absorption and emission lines,

[4]http://www.dwhoard.com/biglist

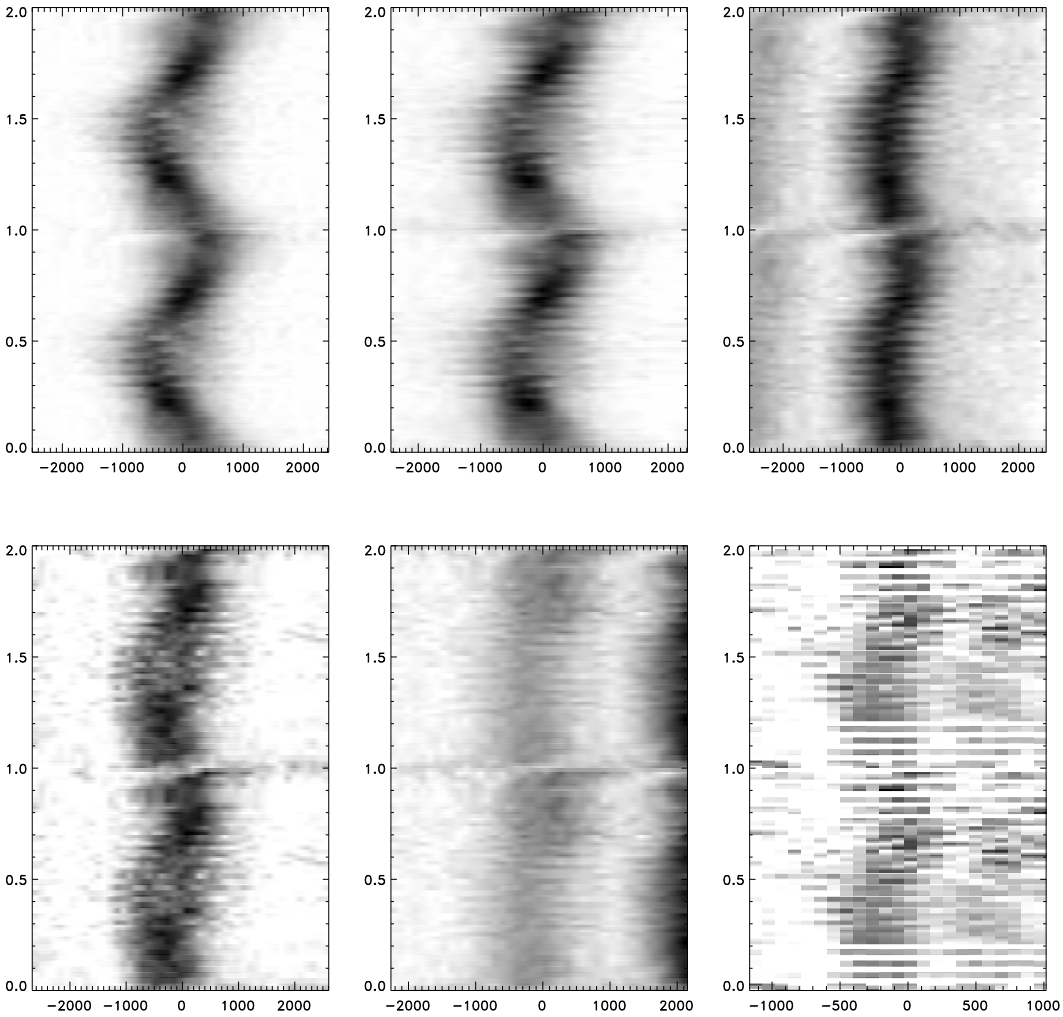

Fig. 6.— Trailed spectra of selected lines of SDSS 0756+0858. 47 spectra obtained on 6 and 7 February 2013 and covering slightly more than two orbital periods were used to construct the images. From the top left to the right in separate panels are presented H_α, H_β and He II, and at the bottom also from the left to right: He I λ4471 Å, complex of fluorescent lines C III/N III and Mg I (inverse gray scale, since the line is in absorption).

often appearing almost featureless. We may assume, that in SDSS 0756+0858 and other SW Sex objects, the accretion disk has a large contribution in the continuum but little in the lines, and that the bright spot is either the only or the dominant source of the emission lines. Thus, the observer of spectral lines "does not see" the presence of the accretion disk and detects only single peaked emission lines from an area known as the bright spot. This can be exacerbated by the elongated down the stream bright spot and the geometrical thickness of disk edges shadowing the emission from its surface.

In fact Dhillon et al. (1997) proposed the exact same idea; they even considered an extended bright spot. But they stopped short affirming presence of such structure in the disk citing an absence of detailed hydrodynamical calculations describing it. Recently, Bisikalo et al. (2008); Kononov et al. (2012) performed such three-dimensional gas-dynamical simulations for accretion disks. Their calculations show the flow of matter in SS Cyg, a dwarf nova with a $\dot{M}\sim\ 8\times10^{-9}\,\mathrm{M}_\odot$/year mass transfer rate, a typical value for dwarf nova. One would expect that the effects obtained in that simulation would get more important with an increase of mass transfer rate. According to their calculations, apart form the stream of matter feeding the

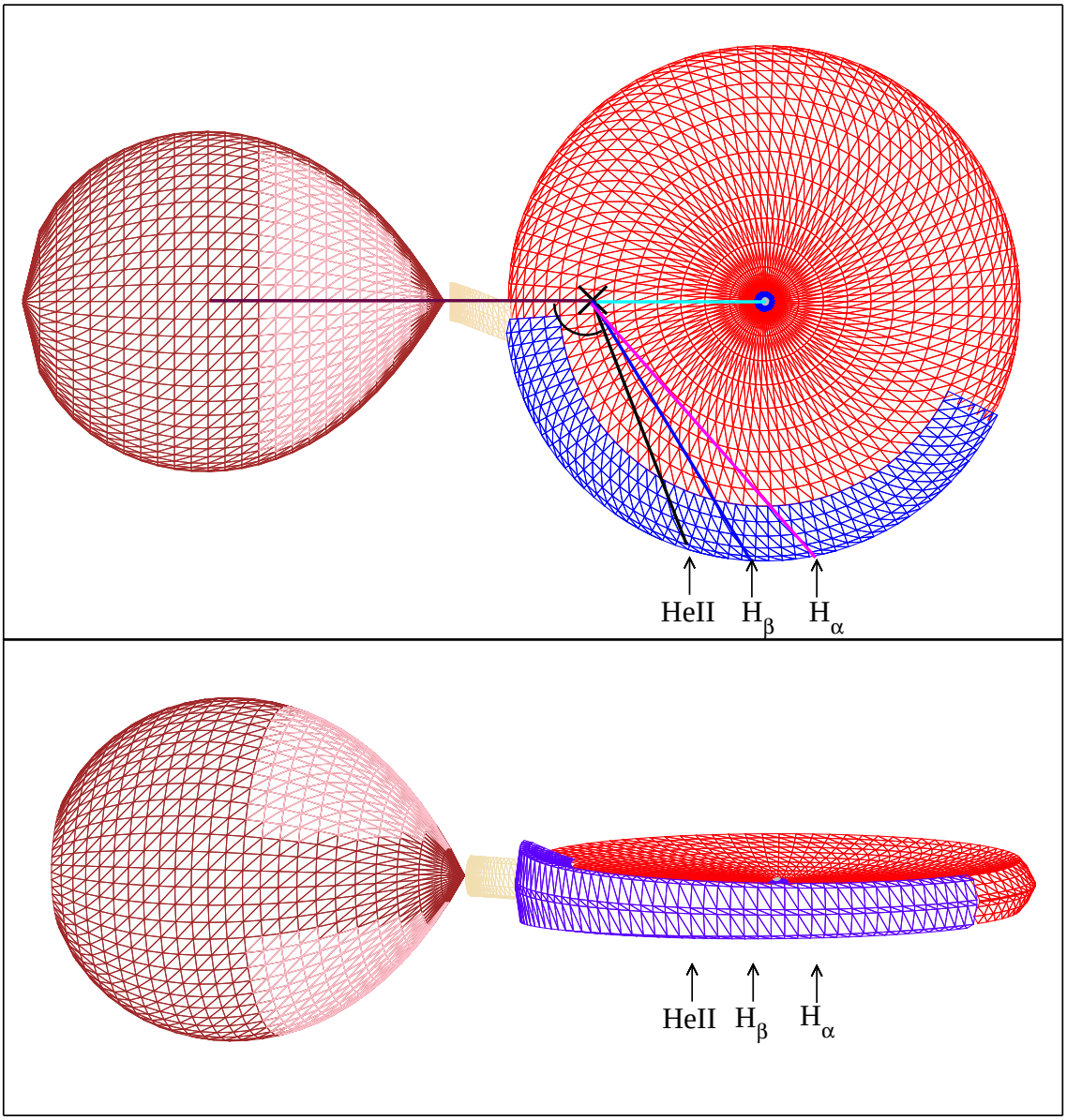

Fig. 7.— SW Sex model. The parameters for this one are selected according to Table 3 to reproduce the light and radial velocity curves closely resembling the observations. The calculated curves are presented in the following figures. The extended hot spot, or hot line is drawn by blue. Marked are the weighted centers of areas where the corresponding emission lines are formed. Because of the temperature gradient in the arc and stratification of lines each of them revolves around the center of mass denoted by "x" with different velocity and phase.

accretion disk from the secondary star, there is an outflow of matter leaving the accretion disk and forming a circum-disk halo. The former apparently plays an important role in SW Sex stars as in all interacting binaries. In this case, its role is enhanced by the extension of the spot into what (Bisikalo et al. 2008) call a "hot line" or arc. Consideration of the latter, i.e. the outflow of matter form the disk, can help to explain the additional features. We can see, in the right panel of Figure 5, that in phase $\phi = 0.5$ the Balmer lines are twice broader than at other phases, but their intensity decreases. They also show irregular variation of width, also called line flaring. This can be explained by the presence of the circum-disk halo which produces lines with broader velocities. It can also be responsible for the appearance of the absorption features. At $\phi = 0.25$ and $\phi = 0.75$ both streams are viewed perpendicular, thus the dispersion of the velocities is smaller and the lines narrower. During the eclipse, the halo remains mostly visible, preventing a total eclipse of the low-excitation lines. The system brightens at $\phi = 0.3 - 0.4$ and exhibits irregular variability, which Dhillon et al. (2013) explain as a non-uniform disc edge. Their model does not explain why it is non-uniform, or why the rim on that side of the disk is not as wide. Knigge et al. (2004) came to a similar conclusion using UV spectra, noting a presence of absorbing material at the phase opposing the eclipse and its nonuniform physical conditions. However if there is outflow, then it will probably introduce a necessary non-uniformity to the disk edge. The flaring of the emission lines has been interpreted as an evidence of magnetic accretion (Rodríguez-Gil et al. 2001; Rodríguez-Gil & Martínez-Pais 2002; Rodríguez-Gil et al. 2009). The claim is supported by evidence of periodic nature of flaring, and in some cases, a more substantial indication is the detection of circular polarization. We do not question presence of magnetic white dwarfs in SW Sex stars and truncation of the accretion disk, but we do not have any manifestation of magnetic field in case of SDSS 0756+0858. We analyzed the equivalent width variability of H_β and He II lines and found no periods except the orbital and an alias related to the exposure length of individual spectra. We also believe that a magnetic accretion modulating the emission lines width would produce substantial X-ray emission, but we detected none.

6. The model

We developed a geometric model of a SW Sex system, presented in Figure 7, to reproduce the observed photometric and spectral features of SDSS 0756+0858. The system is comprised of a primary white dwarf, a secondary red dwarf star; a stream of accretion matter, a thick $z^d(r) = z^d(r_{out})(r/r_{out})^\nu$ accretion disk, and an elongated and extended hot spot/line. The white dwarf is a sphere, defined by the mass-radii relation in Warner (2.83b, Warner 1995). The secondary is assumed to fill its Roche lobe, and the Roche lobe shape is directly calculated using equation 2.2 (Warner 1995) for equipotential $\Phi(L_1)$. The mass and temperature of the primary are defined as initial parameters. The mass of the secondary is obtained from the mass-period relation 2.100 (Warner 1995), which also defines the effective temperature of the secondary, using relations $\log T_2^{\rm eff} \propto \log M_2$ from Malkov (2007). The illumination of the secondary by the primary is also included. A standard temperature gradient

$$T^d(r) \sim T_* \times r^{-3/4},$$

where

$$T_* = \left(\frac{3GM_{wd}\dot{M}}{8\pi\sigma R_{wd}^3} \right)^{1/4}$$

(see 2.35, 2.36,2.37 Warner 1995) between the inner and the outer edges ($r_{out} \approx 0.60a/(1+q)$) of the disk was assumed. The impact of the stream with the outer rim of the disk forms a shock-heated trailing arc along the rim as was described by the schematic model by Hoard et al. (2003, Fig.12 therein) and the hotline defined in Bisikalo et al. (2008). The vertical size $z^{\rm s}$ and the temperature $T^{\rm s}$ of the arc-like hot spot are not uniform; it is wider and hotter at the impact point (φ_{min}) and declines both in temperature and vertical extension, according to an arbitrarily selected manner described by the following equations:

$$T^s(\varphi) = T^d(1.0 + \gamma^T f(\varphi)^{\frac{3}{2}})$$

$$z^s(\varphi) = z^d(1.0 + \gamma^z f(\varphi)^{\frac{5}{2}}),$$

where φ is the angle between the line connecting the stars in conjunction and the direction of the

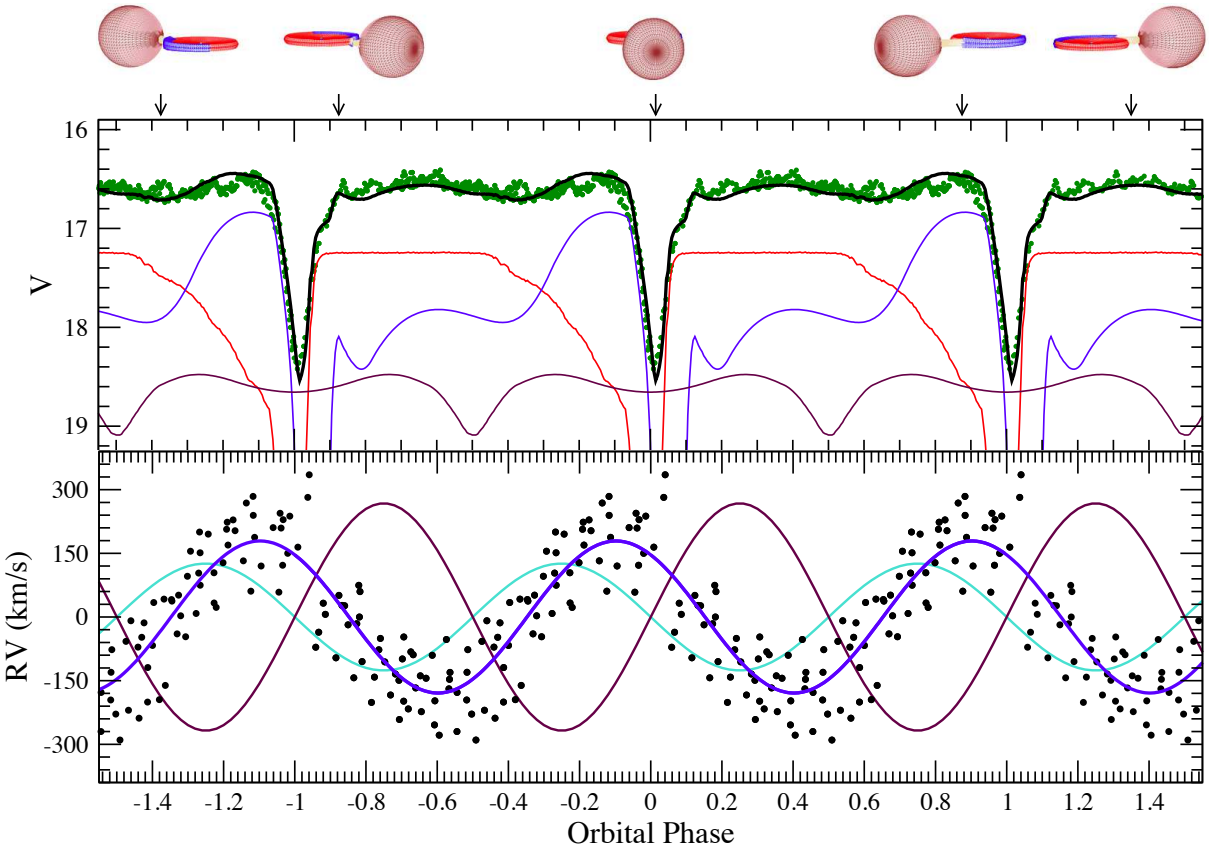

Fig. 8.— Light and radial velocity curves calculated from the model. At the top of the figure five different perspectives of the model are presented. Their corresponding phases are marked by ticks on the outer side of the upper panel. Phase 0.0 in this figure corresponds to the inferior conjunction, unlike previous figures where it corresponded to the eclipse center ($\phi = 0.025$ difference). In the upper panel the computed V-band light curves of the disk (red), the hot spot (blue) and the secondary star (brown) are plotted along the sum of all components, presented as a black line. The green points are observations in V-band. The contribution of white dwarf is negligible and lays out of the figure. In the bottom panel the computed radial velocity of stellar components are presented. The higher velocity brown curve corresponds to the secondary star and the cyan to the white dwarf. They are not observed. The points correspond to the observed radial velocity of He II line and the blue curve is the computed velocity from the model. Two Balmer lines marked in Figure 7 are not presented, not to complicate the plot, but they describe the observed points as good as the He II.

spot viewed from the center of mass; $f(\varphi) \equiv a \times \varphi + b$ is a linear function with constants a and b defined by boundary conditions of $f(\varphi_{min}) = 1$; and $f(\varphi_{max}) = 0$, and γ^T, γ^z are free parameters.

The surface of each component of the system is divided in a series of triangles as shown in Figure 7. We assume that each triangle emits as a blackbody with corresponding temperature. Figure 8 presents geometry snapshots (top) and the model calculations of light and radial velocity curves (bottom two). The light curves of individual components of the binary system were obtained by integrating the emission from all the elements lying in a sight of view and are presented in the middle panel of Figure 8. The flux from the white dwarf is almost totally blocked by the thick disk. Two equally dominant sources of emission from the model light curves are the accretion disk and the bright spot/arc (denoted by the red and blue lines respectively). The disk's contribution is more significant after the eclipse, when the bright spot is largely hidden behind it. In contrast, the form of the light curve before the eclipses, is mostly determined by the bright spot. The eclipse corresponds to the blockage of the bright spot by the secondary. Thus, the observational phase $\phi = 0$, which is assigned to the conjunction of the stellar components, does not coincide with the zero

Table 3: Model parameters used to compute the photometry and radial velocity curves.

System input:	
Period	11834.6 sec
Mass of Primary	$0.6 M_\odot$
mass ratio	0.47
system inclination	84^o
radial disk size r_{out}	$0.40 R_\odot$
vertical disk size $z^d(r_{out})$	$0.10\ R_\odot$
ν radial slope	3
$\dot{M}$	$1.2 \times 10^{-10} M_\odot/yr$
Distance	290 pc
Hot spot/line:	
width	$0.2 \times r_{out}$
length	140^o
γ^T	0.75
γ^z	0.75
System output:	
Mass of Secondary	$0.28 M_\odot$
T_2	$3250\ K$
a separation	$1.07\ R_\odot$

phase in Figure 8. The fit is not optimized mathematically, but it is sufficient to explain all the observed features: the eclipse, the pre-eclipse-hump, the depression around phase 0.6-0.7, and even the little wiggle at $\phi = 0.18$ reasonably well. The main parameters of the model are given in Table 3. We can achieve satisfactory qualitative resemblance between the modeled light curves and the observations by simply varying the system inclination and the hot spot parameters. All other parameters are fixed.

The model describes also quite well the RV amplitude and phase of the emission lines as basically emanating from the hot spot. Since the hot spot is extended, and its temperature is the highest at the impact point, there is a stratification of temperatures and hence the excitation levels along the arc. The lines of different excitation energies are predominantly formed at a different angles from the mass center, as marked in Figure 7. He II arises from an area located the closest to the the center of mass of the binary and thus, has the lowest amplitude of the radial velocity. The lower the excitation level, the further is the weighted center of the line forming region along the arc, and, therefore, the larger is the radial velocity amplitude. The phasing of the lines relative to the orbital phase changes accordingly. In the bottom panel of Figure 8 the calculated radial velocity curve for He II line is presented and it excellently describes points obtained from the observations. Also shown are calculated velocities of stellar components, which are not observed. Calculated velocities of Balmer lines are not presented, so as not to crowd the figure.

The model also is able to describe fine details, in particular, what happens at the phases $\phi = 0.9$ to 1.0. The white dwarf (and the accretion disk in general) has already reached the maximum positive velocity and it is moving toward stellar conjunction with decreasing radial velocity (light blue curve). But emission lines, formed predominantly in the bright arc still have an increasing radial velocity peaking around phase $\phi = 0.9$ (blue curve). Around that phase, however, the secondary starts eclipsing part of the bright arc where the matter with the growing velocities is concentrated, and the observer sees only the far extreme of the arc, which moves in the opposite direction. Thus, for a brief moment before the total eclipse of the bright arc, we detect a less intense emission line with decreasing RV. This creates a zig-zag in the trailed spectra (see Figure 6). The zig-zag is best pronounced in the He II line, since it is formed closer to the stream/dick impact point, which is eclipsed first, leaving rest of the arc visible. At the depth of the eclipse ($\phi = 0.025$ in phases determined by radial velocities), the very tip of the retreating half of the disk or the hot arc is still visible (see the cartoon at the top of the Figure 8). It contains matter moving away from the observer with the sum of Keplerian and orbital velocities, and appears in the RV curves and trailed spectra as a high velocity tail. This model does not take into account the matter outflowing from the opposite side of the hot arc side in the disk. We think that the inclusion of that element would allow fine tuning of the model to the observations.

7. Conclusions

We have unveiled a new eclipsing SW Sex star. It has an orbital period 3.287 hr, at the centre of a range of periods where the great majority of SW Sex stars cluster. It has all observational characteristics of this type of stars and, as such, increases the number of eclipsing systems of this

particular type at these periods. We believe that this clustering is something not well understood and should be addressed, but it is beyond the scope of this study. On the other hand we have been able to reproduce the photometric and radial velocity curves of SDSS 0756+0858 by simply assuming that the emission lines are predominantly formed/observed from the hot, extended spot, without the additional speculative mechanisms proposed in other models. We think that the absence of lines from other parts of the disk is a consequence of a disk having a high temperature and a surface density regime, and partially due to self obscuration by the thick rim at the same time. We also, believe that there is an outflow of matter from the opposite to the arc side of the disk, where the absorption features observed in SW Sex objects are formed. That outflowing matter may also contribute to the high velocity components of the low-excitation lines.

MSH and DGB is grateful to CONACyT for grants allowing their post-graduate studies. GT and SZ acknowledge PAPIIT grants IN-109209/IN-103912 and CONACyT grants 34521-E; 151858 for resources provided toward this research. We would like to thank the *Swift* team for opportunity to observe the object and their prompt response to our application. Our thanks to Dr. J. Echevarria for reading the article and for his critical and helpful comments.

REFERENCES

Araujo-Betancor, S., Knigge, C., Long, K. S., et al. 2003, ApJ, 583, 437

Bisikalo, D. V., Kononov, D. A., Kaigorodov, P. V., Zhilkin, A. G., & Boyarchuk, A. A. 2008, Astronomy Reports, 52, 318

Dhillon, V. S., Marsh, T. R., & Jones, D. H. P. 1991, MNRAS, 252, 342

Dhillon, V. S., & Rutten, R. G. M. 1995, MNRAS, 277, 777

Dhillon, V. S., Marsh, T. R., & Jones, D. H. P. 1997, MNRAS, 291, 694

Dhillon, V. S., Smith, D. A., & Marsh, T. R. 2013, MNRAS, 428, 3559

Hellier, C. 2000, New A Rev., 44, 131

Hoard, D. W., Szkody, P., Still, M. D., Smith, R. C., & Buckley, D. A. H. 1998, MNRAS, 294, 689

Hoard, D. W., Szkody, P., Froning, C. S., Long, K. S., & Knigge, C. 2003, AJ, 126, 2473

Hoare, M. G. 1994, MNRAS, 267, 153

Honeycutt, R. K., Schlegel, E. M., & Kaitchuck, R. H. 1986, ApJ, 302, 388

Khruzina, T., Dimitrov, D., & Kjurkchieva, D. 2013, A&A, 551, A125

Knigge, C., Araujo-Betancor, S., Gänsicke, B. T., et al. 2004, ApJ, 615, L129

Kononov, D. A., Giovannelli, F., Bruni, I., & Bisikalo, D. V. 2012, A&A, 538, A94

Malkov, O. Y. 2007, MNRAS, 382, 1073

Oke, J. B. 1990, AJ, 99, 1621

Rappaport, S., Verbunt, F., & Joss, P. C. 1983, ApJ, 275, 713

Rodríguez-Gil, P., & Martínez-Pais, I. G. 2002, MNRAS, 337, 209

Rodríguez-Gil, P., Casares, J., Martínez-Pais, I. G., Hakala, P., & Steeghs, D. 2001, ApJ, 548, L49

Rodríguez-Gil, P., Gänsicke, B. T., Hagen, H.-J., et al. 2007b, MNRAS, 377, 1747

Rodríguez-Gil, P., Schmidtobreick, L., Gänsicke, B. T. 2007a, MNRAS, 374, 1359

Rodríguez-Gil, P., Martínez-Pais, I. G., & de la Cruz Rodríguez, J. 2009, MNRAS, 395, 973

Schmidtobreick, L. 2012, arXiv:1211.2171

Schwarz, U. J. 1978, A&A, 65, 345

Szkody, P., Piche, F., & Feinswog, L. 1990, ApJS, 73, 441

Szkody, P., Anderson, S. F., Brooks, K., et al. 2011, AJ, 142, 181

Thorstensen, J. R., Ringwald, F. A., Wade, R. A., Schmidt, G. D., & Norsworthy, J. E. 1991, AJ, 102, 272

Tout, C. A., Pringle, J. E., & La Dous, C. 1993, MNRAS, 265, L5

Yakin, D. G., Suleimanov, V. F., Vlasyuk, V. V., & Spiridonova, O. I. 2013, Astronomy Letters, 39, 38

Warner, B. 1995, Cambridge Astrophysics Series, 28

White, J. C., II, Schlegel, E. M., & Honeycutt, R. K. 1996, ApJ, 456, 777

Williams, R. E. 1989, AJ, 97, 1752

Wynn, G. A., & King, A. R. 1995, MNRAS, 275, 9

This 2-column preprint was prepared with the AAS LaTeX macros v5.2.